HHS Public Access

Author manuscript

Neuroimage. Author manuscript; available in PMC 2015 October 15.

Published in final edited form as:

Neuroimage. 2014 October 15; 100: 244–253. doi:10.1016/j.neuroimage.2014.06.009.

Axonal transport rate decreased at the onset of optic neuritis in EAE mice

Tsen-Hsuan Lin[1,*], **Joong Hee Kim**[2], **Carlos Perez-Torres**[2], **Chia-Wen Chiang**[3], **Kathryn Trinkaus**[4], **Anne H. Cross**[5,6], and **Sheng-Kwei Song**[2,6]

[1]Department of Physics, Washington University, St. Louis, MO 63130, USA

[2]Department of Radiology, Washington University School of Medicine, St. Louis, MO 63110, USA

[3]Department of Chemistry, Washington University, St. Louis, MO 63130, USA

[4]Divison of Biostatistics, Washington University School of Medicine, St. Louis, MO 63110, USA

[5]Department of Neurology, Washington University School of Medicine, St. Louis, MO 63110, USA

[6]Hope Center for Neurological Disorders, Washington University School of Medicine, St. Louis, MO 63110, USA

Abstract

Optic neuritis is frequently the first symptom of multiple sclerosis (MS), an inflammatory demyelinating neurodegenerative disease. Impaired axonal transport has been considered as an early event of neurodegenerative diseases. However, few studies have assessed the integrity of axonal transport in MS or its animal models. We hypothesize that axonal transport impairment occurs at the onset of optic neuritis in experimental autoimmune encephalomyelitis (EAE) mice. In this study, we employed manganese-enhanced MRI (MEMRI) to assess axonal transport in optic nerves in EAE mice at the onset of optic neuritis. Axonal transport was assessed as (a) optic nerve Mn^{2+} accumulation rate (in % signal change/hour) by measuring the rate of increased total optic nerve signal enhancement, and (b) Mn^{2+} transport rate (in mm/hour) by measuring the rate of change in optic nerve length enhanced by Mn^{2+}. Compared to sham-treated healthy mice, Mn^{2+} accumulation rate was significantly decreased by 19% and 38% for EAE mice with moderate and severe optic neuritis, respectively. The axonal transport rate of Mn^{2+} was significantly decreased by 43% and 65% for EAE mice with moderate and severe optic neuritis, respectively. The degree of axonal transport deficit correlated with the extent of impaired visual function and diminished microtubule-associated tubulins, as well as the severity of inflammation, demyelination, and axonal injury at the onset of optic neuritis.

Corresponding Author, Sheng-Kwei "Victor" Song, Ph.D., Biomedical MR Laboratory, Campus Box 8227, Washington University School of Medicine, Room 2313, 4525 Scott Ave, St Louis, MO 63110, USA, Fax: +1 314 362 0526, Phone: +1 314 362 9988, ssong@wustl.edu.

*Current Address: Institute of Biomedical Sciences, Academia Sinica, Taipei City 11529, Taiwan (R.O.C.)

Introduction

Multiple sclerosis (MS) is a common inflammatory demyelinating disorder of the central nervous system (CNS) causing significant neurological dysfunction that accumulates over a lifetime (Compston and Coles, 2008; Trapp and Nave, 2008). Experimental autoimmune encephalomyelitis (EAE) is a widely used animal model of MS exhibiting many MS-like neurological dysfunctions including optic neuritis (ON) (Bettelli et al., 2003; Shao et al., 2004), which is often an early symptom of MS (Beck et al., 1993; Beck et al., 2003; Pascual et al., 2009; Shams and Plant, 2009). Inflammatory demyelination and axonal injury in the optic nerve that are commonly seen in MS patients are also frequently present in EAE-affected mice (EAE mice) (Diem et al., 2008; Gold et al., 2006; Sun et al., 2007). Accumulation of amyloid precursor protein (APP) is regarded as an early marker of axonal injury in MS patients and EAE mice (Bitsch et al., 2000; Fairless et al., 2012; Ferguson et al., 1997; Linker et al., 2010; MacKenzie-Graham et al., 2012; Petratos et al., 2012). Interruption of axonal transport in injured axons results in the accumulation of APP, which can be detected by immunohistochemistry (IHC) (Ferguson et al., 1997; Smith et al., 2003). Hence, axonal transport disruption could be an early event in EAE and in some patients with MS. However, few reports have assessed axonal transport in MS or its EAE models.

Manganese-enhanced MRI (MEMRI) has been applied in the rodent CNS (Bearer et al., 2007; Chan et al., 2011; Olsen et al., 2010; Pautler et al., 1998; Thuen et al., 2008) to investigate ion homeostasis and axonal transport. Manganese ion (Mn^{2+}), as a calcium analogue, is taken up by neurons through voltage-gated Ca^{2+} channels. In the mouse visual system, Mn^{2+} is taken up by retinal ganglion cells, packaged in vesicles, and transported along microtubules down the axonal tract (Pautler and Koretsky, 2002). As a paramagnetic ion, Mn^{2+} reduces tissue water T1 relaxation time and its presence in tissues can be identified as hyper-intensities in the T1W image (Silva et al., 2004). Recently, MEMRI has been applied to examine pathologies of the optic nerve, including blood-brain barrier integrity or inflammation, in EAE rats and mice (Boretius et al., 2008; Gadjanski et al., 2009; Guy, 2008). In this study, MEMRI was further extended as a dynamic tracer to investigate *in vivo* axonal transport integrity assessing axonal transport rates quantitatively. Our results support that axonal transport impairment is present at the onset of optic neuritis in EAE mice, and correlates with impaired visual function and the underlying optic nerve pathologies. To the best of our knowledge, this is the first quantification of axonal transport rate in optic nerve of EAE mice at the onset of optic neuritis. Our finding directly validated the previous axonal transport rate assessed by Mn^{2+}-accumulation. We believe that the current report may provide a critical link between previous and future MEMRI assessed axonal transport rate in mice.

Materials and Methods

All experimental procedures involving animals were approved by Washington University's Animal Studies Committee and conformed to the Public Health Service Policy on Humane Care and Use of Laboratory Animals (http://grants.nih.gov/grants/olaw/olaw.htm).

Experimental autoimmune encephalomyelitis (EAE)

Sixteen 7-week old C57BL/6J mice were obtained from Jackson Laboratory (Bar Harbor, ME, USA). Ten mice were randomly selected to be immunized with 50 μg $MOG_{35–55}$ peptide emulsified (1:1) in incomplete Freund's adjuvant (IFA) and Mycobacterium tuberculosis. Pertussis toxin (300 ng; PTX, List Laboratories, Campbell, CA, USA) was injected intravenously on the day of $MOG_{35–55}$ immunization and two days later. The remaining six sham mice underwent the same immunization procedure with only IFA without $MOG_{35–55}$. Mice were assessed daily for neurological disabilities using a standard clinical score (CS) system: 1 = limp tail; 2 = hind limb weakness sufficient to impair righting; 3 = one limb paralyzed; 4 = two limbs paralyzed; 5 = 3 or more limbs paralyzed or the animal is moribund (mice were euthanized if they reach grade 5).

Visual acuity (VA)

The VA of mice was measured daily starting before immunization using the Virtual Optometry System (Optomotry, Cerebral Mechanics, Inc., Canada). Briefly, the virtual rotating columns were projected on the LCD monitors with different spatial frequencies in cycles/degree (c/d). The mouse head movement in response to the virtual column rotations was noted. The spatial frequency was increased starting from 0.1 c/d with step size of 0.05 c/d until the mouse stopped responding. The VA was defined as the highest spatial frequency of the virtual rotating columns to which the mouse was able to respond. We have previously reported that VA of normal C57BL/6 mice to be 0.38 ± 0.03 c/d (mean ± SD, n=30) and defined VA ≤ 0.25 c/d as the onset of acute ON for EAE mice (Chiang et al., 2012). MEMRI was performed on the day when mice exhibited VA ≤ 0.25 c/d. The mice in sham group did not develop impaired visual function and underwent the same MEMRI procedure at the same day as EAE group.

Intravitreal $MnCl_2$ injection

$MnCl_2$ was injected in the eye that had a measured VA ≤ 0.25 c/d. Mice were anesthetized using 1.5-2% isoflurane/oxygen. After the appropriate level of anesthesia was achieved, assessed by the lack of response to toe pinch, mice were placed on a custom-made head holder. A 34-gauge needle, connected to a micro-injection pump (WPI Instrument, FL, US), was inserted into the posterior vitreous at 1–1.3 mm posterior to limbus. A dose of 50 nmol $MnCl_2$, given as 0.25 μL of 0.2 M solution (Bearer et al., 2007), was delivered at a rate of 3 μL/min. At the conclusion of injection, the needle was left in the place for an extra 1 minute before withdrawal and then a drop of antibiotic gel was applied to both injected and un-injected eyes (Chen et al., 2012; Lin et al., 2014).

Manganese-enhanced MRI (MEMRI)

MEMRI was performed immediately after $MnCl_2$ administration on a 4.7 T Agilent DirectDrive small-animal MRI system (Agilent Technologies, Santa Clara, CA) equipped with Magnex/Agilent HD image gradient coil (Magnex, Oxford, UK) with pulse gradient strength up to 58 G/cm and a gradient rise time ≤ 295 μs. Mice were anesthetized by 1.5% isoflurane/oxygen. During experiments, respiratory rate and body temperature were monitored using a MR compatible animal monitoring system (SA Instrument, Inc., Stony

Brook, NY, US) and maintained at 130 – 150 breaths/min and 37°C with a regulated circulating warm water pad underneath mouse body along with regulated warm air blown into the magnet bore, respectively. A pair of 8-cm diameter volume (transmit) and 1.7-cm diameter surface (receive) active-decoupled coils were used.

A standard 3D gradient echo sequence was employed for T1-weighted (T1W) image of the whole mouse brain with the following parameters: repetition time (TR) = 15 ms, echo time (TE) = 2.63 ms, flip angle = 20°, number of averages = 16, field-of-view (FOV) = 15 × 15 × 22 mm^3, matrix size = 128 × 128 × 64 (zero-filled to 256 × 256 × 128), acquisition time = 32.8 minutes. Ten successive sets of 3D-T1W image were captured approximately from 0.55 – 5.5 hours post-injection.

B1-inhomogeneity correction

A 3D-T1W image of a phantom (uniform 13 × 9 × 25 mm^3 of 2% agar gel placed underneath the active-decoupled surface coil with the distance between gel and coil similar to the *in vivo* study) was acquired using the same MEMRI parameters with 64 averages to obtain the profile of surface coil sensitivity (acquisition time was 131.2 minutes). To correct B1 inhomogeneity, the raw 3D-T1W image of the mouse brain was divided by the 3D-T1W image of 2% agar phantom voxel by voxel directly using image calculator in ImageJ (Schneider et al., 2012) and the corrected 3D-T1W image data set was generated for analyzing MEMRI data.

MEMRI data analysis

Surface-coil sensitivity profile corrected T1W image data set of the final time point was displayed using volume viewer plugin version 1.31 in ImageJ (http://rsbweb.nih.gov/ij/plugins/volume-viewer.html, NIH, US) with z-aspect factor of 2 resulting in isotropic 256 × 256 × 256 data matrix. The 3D data matrix was adjusted by rotating about x- and z-axis and distance slider to make oblique image plan bisecting both optic nerves. The oblique image containing both nerves was saved and converted to 8-bit gray scale. The corrected 3D-T1W image data sets of other previous time points were rotated using the same rotation parameters. The final result was a stack of oblique corrected T1W images (ten images) from each mouse (from 0.55 – 5.5 hours post-injection) for accumulation and transport rate calculation.

To derive the rate of total Mn^{2+} accumulation, ROI of optic nerves were drawn on the oblique corrected T1W image for each mouse. The average size of the optic nerve ROI was 188 ± 27 voxels (n=160, mean ± SD). A 20 × 20-voxel reference area ROI was drawn 30 voxels away from optic nerve head. This reference area ROI was pure muscle, not affected by intravitreal Mn^{2+} loading. The ROI information of optic nerves and reference area was saved and then applied to oblique corrected T1W images of other previous time points. Finally, the normalization was performed by taking the ratio of signal intensity of optic nerve ROIs and their respective reference ROI.

To calculate Mn^{2+} transport rate, a line ROI was drawn along the signal-enhanced and the contralateral optic nerves at the final time point, taking advantage of the increased contrast

for the ROI definition. The same line ROIs were applied to the corrected T1W images. The average size of Mn^{2+}-loaded and reference line ROI was 54 ± 3.3 and 53 ± 3.2 voxels (n = 160, mean ± SD) respectively. The arrival of Mn^{2+} at the loaded nerve was defined by counting voxels with the signal intensity ≥ mean + 2 SD of the signal intensity of the contralateral optic nerve. After determining the number of voxels in the length of Mn^{2+}-enhanced optic nerves was converted to millimeter by combining the known in-plane image resolution, the geometric transformation associated with the oblique slice plane and the Pythagorean equation (Sally and Sally, 2007). Transport rate was defined as the slope of Mn^{2+}-enhanced length over time by linear fitting.

Immunohistochemistry (IHC) of optic nerves

Following MEMRI experiments, mice underwent intra-cardiac perfusion with 1% phosphate buffered saline (PBS, pH = 7.4) followed by 4% paraformaldehyde in 0.01 M PBS. Brains were excised and post-fixed in the same fixative for 24 hours then transferred to 0.01 M PBS for storage at 4 °C until histological analysis was performed. Mouse optic nerves were dissected from each brain and embedded in 2% agar blocks (Blewitt et al., 1982). Then, the agar blocks were embedded in paraffin wax and 5-μm thick transverse slices were sectioned for IHC staining. Sectioned slices were deparaffinized, rehydrated, and blocked using solution mixed with 1% bovine serum albumin (BSA, Sigma-Aldrich, MO, USA) and 5% normal goat-serum solution (Invitrogen, CA, USA) for 20 minutes at room temperature to prevent non-specific binding and to increase antibody permeability. Slides were incubated with monoclonal antiphosphorylated neurofilament antibody (SMI-31; 1:1000, Covance, NJ, USA) to stain noninjured axons, or with rabbit anti-myelin basic protein antibody (MBP, 1:1000, Sigma-Aldrich, MO, USA) to stain myelin sheath (Budde et al., 2009; Song et al., 2003; Sun et al., 2007), or monoclonal microtubule-associated βIII tubulin (TUJ1, 1: 1500, Covance, IN, USA) to stain base structure of motor protein movement at 4°C overnight. After rinsing, goat anti-mouse IgG or goat anti-rabbit IgG conjugated Alexa 488 (1:800, Invitrogen, CA, USA) were applied to visualize immunoreactivity of phosphorylated neurofilaments and MBP. Finally, slides were covered using Vectashield Mounting Medium with 4',6-diamidino-2-phenylindole (DAPI) (Vector Laboratory, CA, USA) to stain nuclei (Budde et al., 2009; Wang et al., 2011). Histological slides were examined with Nikon Eclipse 80i fluorescence microscope equipped with a 60× water objective, and images were captured with a black-and-white CCD camera using MetaMorph software (Universal Imaging Corporation, Sunnyvale, CA, USA) at the center of optic nerve.

Histological data analysis

The whole field of SMI-31, MBP, TUJ1, and DAPI staining images at 60× magnification were captured with the same fluorescence light intensity and exposure time. All captured images were converted to 8- bit gray scale and analyzed using threshold, analyze particles and gray level watershed segmentation functions in ImageJ (http://bigwww.epfl.ch/sage/soft/watershed/).

Statistical analysis

Linear repeated measures models were used to test normalized Mn^{2+}-enhancement signal intensities at each time point (from 0.55 – 5.5 hours post-injection with 0.55-hour step size)

for pairwise comparison among shame and EAE mice with moderate and severe ON: sham vs. moderate, sham vs. severe, and moderate vs. severe groups.

Multiple comparisons for accumulation rate, transport rate, TUJ1, SMI-31, MBP, and DAPI by each study group (sham/moderate/severe) were performed using a linear regression model of each outcome. P-values for the three pairwise tests (sham vs. moderate, sham vs. severe, and moderate vs. severe) were adjusted using Tukey's HSD (honest significant difference). The correlation coefficients for accumulation or transport rate with each TUJ1, SMI-31, MBP, and DAPI or for accumulation rate with transport rate were analyzed by Spearman's rank correlation coefficient, which includes one observation per mouse (independent assumption was met).

Results

Visual acuity

After immunization, daily visual acuity (VA) of sham and EAE mice was measured. When mice exhibited VA ≤ 0.25 c/d (Chiang et al., 2012), MEMRI was performed (12 ± 2.1 days post-immunization, mean ± SD, n=10). In this study, CS appeared in some EAE mice at the same day as the first sign of impaired VA. VA at ON onset was different among mice examined and was used to separate mice into three groups: sham (VA = 0.35 or 0.4 c/d; CS = 0), moderate ON (VA = 0.2, CS = 1 for one mouse; VA = 0.25 c/d, CS = 0 for the rest four mice), and severe ON (VA = 0 c/d, CS =0 for two mice and CS = 2.5 for the rest 3 in this group; Fig. 1A).

The optic nerve Mn^{2+} accumulation rate

Since the image intensity was used to detect Mn^{2+} arrival, the B1-inhomogeneity correction of the surface coil was performed (Lin et al., 2003, Hou, 2006) using the 3D T1W image of 2% agar gel (Fig. 2). After correction, the averaged intensity of randomly selected line profiles on the corrected T1W images was comparable in both vertical and horizontal directions suggesting a reasonable B1-field inhomogeneity correction (Fig. 2D and 2E).

A series of time-lapse representative B1-profile corrected oblique T1W images of sham, moderate and severe ON mice exhibited different degrees of Mn^{2+}-enhancement suggesting different axonal transport rates in optic nerves. The hyper-intensity of optic nerve resulting from axonal transport of Mn^{2+} was readily visible (Fig. 1B). The optic-nerve and reference ROI were defined (Fig. 3A). The time course of group averaged signal intensity ratios of optic-nerve to reference ROI exhibited different rate of signal enhancement among the sham and EAE mice with moderate and severe ON (Fig. 3B). The accumulation rate of Mn^{2+} in the optic nerve was defined as the slope of the linear fit of the data over time. The group averaged optic nerve Mn^{2+} accumulation rate (the slopes) of sham, moderate ON, and severe ON mice was 0.16, 0.13, and 0.10 a.u./hour, respectively (Table 1; Fig. 3C). The accumulation rate in EAE mice was significantly slower than that of the sham by 19% (moderate ON, $p < 0.005$), and 38% (severe ON, $p < 0.005$). The accumulation rate was 23% ($p < 0.05$) slower in the EAE mice with severe ON than that with the moderate ON. The accumulation rate correlated with VA ($r = 0.87$, $p < 0.0001$, data not shown).

Transport rate of Mn^{2+}

The Mn^{2+}-loaded and contralateral optic nerve reference line ROIs were defined (Fig. 4A). The enhanced T1W intensity of the optic nerve after Mn^{2+} loading was readily discernible after the subtraction of mean line ROI intensity of the reference optic nerve (Fig. 4B – 4D). Representative difference images of sham and EAE mice with moderate ON exhibited different length of the Mn^{2+}-enhanced optic nerve. The entire optic nerve was enhanced at 3.3 and 5.5 hours post-injection for sham (Fig. 4B) and EAE mice with moderate ON (Fig. 4C), respectively. In EAE mice with severe ON, only partially enhanced optic nerve was seen (Fig. 4D). The time course suggested that the group-averaged time to enhance the entire optic nerve took 3.3 and 4.95 hours for sham and EAE mice with moderate ON, respectively (Fig. 4E). The slope of each group represents the transport rate (% of optic nerve/hour). The group averaged Mn^{2+} transport rate of sham, moderate ON, and severe ON mice was 26, 14, and 8 % of optic nerve/hour (Fig. 4E). The Mn^{2+} transport rate converted to mm/hour was: 0.92, 0.52, and 0.32 mm/hour for the sham, moderate ON, and severe ON mice, respectively (Table 1). The transport rate of EAE mice was decreased compared with sham mice by 43% ($p < 0.05$) and 65% ($p < 0.005$) respectively for moderate and severe ON groups. EAE mice with moderate ON exhibited a nonsignificant trend of faster transport rate than severe ON mice ($p = 0.15$). The transport rate correlated well with the VA ($r = 0.85$, $p < 0.0001$, data not shown).

Immunohistochemistry (IHC) of optic nerve

Post-image TUJ1, SMI-31, MBP, and DAPI staining of optic nerves from sham and EAE mice with moderate and severe ON was used to assess the integrity of microtubules, axons myelin sheaths, and the extent of cellularity (Fig. 5A). Increased number of DAPI positive nuclei in EAE optic nerves was observed (Fig. 5A). The positive TUJ1 stains significantly decreased in optic nerves from the severe EAE mice ($4.2 \pm 1.3 \times 10^5$, $p = 0.006$, Fig. 5B), insignificantly decreased in moderate EAE ($4.9 \pm 1.4 \times 10^5$, $p = 0.059$, Fig. 5B), when comparing to the sham group ($6.5 \pm 0.7 \times 10^5$). The SMI-31 positive axon counting showed a significantly diminished intact axon density in optic nerves from EAE mice with moderate ($5.6 \pm 0.5 \times 10^5$, $p < 0.005$, Fig. 5B) and severe ($4.5 \pm 0.9 \times 10^5$, $p < 0.005$, Fig. 5B) ON. The significant loss of MBP positive axons expressed as area fraction in optic nerves with moderate (41.6 ± 2.0 %, $p < 0.05$, Fig. 5B) and severe (34.0 ± 3.4 %, $p < 0.005$, Fig. 5 B) ON was also observed compared with the sham group (48.3 ± 3.9 %). DAPI positive cell nuclear staining was significantly increased in optic nerves from mice with severe ON ($9.1 \pm 3.3 \times 10^3$) when compared with the sham ($3.9 \pm 0.6 \times 10^3$, $p < 0.005$, Fig. 5B) and moderate ON ($5.4 \pm 1.0 \times 10^3$, $p < 0.05$, Fig. 5 B) mice. However, the difference between sham ($3.9 \pm 0.6 \times 10^3$) and mice with moderate ON ($5.4 \pm 1.0 \times 10^3$, $p = 0.1$, 5B) was not significant. The Mn^{2+} accumulation rate correlated well with Mn^{2+} transport rate ($r = 0.78$, $p = 0.0003$, Fig. 6A). The Mn^{2+} accumulation and transport rate correlated well with the extent of TUJ1-positive microtubule-associated tubulin integrity ($r = 0.68$ and $r = 0.76$, respectively, $p < 0.005$), intact axonal density ($r = 0.85$ and $r = 0.86$, respectively, $p < 0.0001$) assessed by the density of SMI-31 positive axons, myelin injury ($r = 0.91$ and $r = 0.82$, respectively, $p < 0.0001$) assessed by the MBP positive axons, and inflammation ($r = -0.83$ and $r = -0.84$, respectively) assessed by the density of DAPI-positive nuclear staining (Fig. 6A – 6I).

Discussion

In this study, we assessed VA by optokinetic response (Fig. 1A) and quantified axonal transport in optic nerves using MEMRI in EAE mice at the onset of ON (Fig. 1B). The rate of Mn^{2+} transport in EAE-affected optic nerves was significantly impaired (Figs. 1, Fig. 3 and 4) indicating defective fast axonal transport at the onset of ON (Millecamps and Julien, 2013). Immunohistochemistry of these tissues also indicated the presence of microtubule impairment, demyelination, inflammation, and axonal injury in optic nerves with ON (Fig. 5B). Each of these axonal pathologies correlated well with decreased axonal transport rate.

The rate of axonal Mn^{2+} accumulation has been reported to reflect axonal transport in mice (Massaad et al., 2010; Sharma et al., 2010; Smith et al., 2007; Wang et al., 2012). In the literature, a linear fit of the MEMRI data over a short time course (< 1 hour) was commonly employed. In this study, a 5.5-hour time course was pursued. A linear repeated measures model accounting for the correlation between observations over time applied to the serial 10 measurements suggested that a linear fit was reasonable (data not shown). Thus, a more complex modeling (Cross et al., 2008; Olsen et al., 2010) was not pursued in this study to analyze the MEMRI time course data. In addition to this widely employed Mn^{2+} accumulation rate, the current study also assessed axonal transport rate in optic nerves at the onset of ON caused by EAE. The reported fast axonal transport rate ranges between 3 – 16 mm/hour (De Vos et al., 2008; Millecamps and Julien, 2013). The Mn^{2+} transport rate by MEMRI has been reported ranging between 0.64 – 5 mm/hour, estimated by a two-point time-lapse measurement (Bearer et al., 2007; Chan et al., 2008; Leergaard et al., 2003; Pautler et al., 1998; Saleem et al., 2002; Van der Linden et al., 2002; Watanabe et al., 2004). In the present study, the Mn^{2+} transport rate in sham optic nerves was 0.92 ± 0.14 mm/hour, at the lower end of published values. Animals in the current study were under isoflurane anesthesia throughout the course of the measurements. The lower axonal transport rate estimated herein may result from the long period of anesthesia (Jevtovic-Todorovic et al., 2013; Kameyama et al., 1999). The transport rate estimated using data from the initial 0.55 hours, i.e., less severely affected by anesthesia, was 1.33, 1.49, and 1.31 mm/hour in sham, moderate and severe ON groups, respectively. The higher initial rate supported the possible effect of prolonged anesthesia on the measured transport rate. The varied rate of transport using the initial time-lapse data immediately after injection may reflect the variable severity of ON among mice, or the variable response of individual mice to the induction of anesthesia, masking the transport rate difference among groups. The linear increase over time of MEMRI length of the optic nerve between 0.55 – 5.5 hours from all groups suggested that a steady-state of anesthesia was reached 0.55 hours after the injection of Mn^{2+}.

The axonal Mn^{2+} transport rate between moderate and severe ON groups was not statistically different (Fig. 3F). This may be due to the variation in axonal pathologies of the severe ON group, leading to a high variance in that group. It may also be due to imprecision of the method of VA measurement (Ridder and Nusinowitz, 2006). Optic nerves from three EAE mice with severe ON were not fully enhanced at the end of 5.5 hours post-injection (Fig. 3 E) while the rest two exhibited whole optic nerve enhancement at 4.4 and 4.95 hours. These two mice also exhibited axonal injury (25% decrease in SMI-31 staining compared

with the control) comparable to that in the moderate ON mice (22 ± 7%). IHC results indicated that the mice with higher transport rates suffered less axon and myelin damage than those with slower transport rates. It is possible that acute vasogenic edema at the ON onset impeded action potential propagation and thus reduced VA without significant axonal pathologies (Guy, 2008; Hickman et al., 2004). It is also worth noting that VA was employed herein to serve as a "clinical" sign of optic neuritis in EAE mice because the conventional clinical score reflecting spinal cord injury does not correspond to visual functions. The mechanistic correlation between VA and the axonal transport remains to be elucidated. One obvious link would be that the impaired axonal transport causes axonal injury leading to visual function impairment (which may or may not be directly reflected by VA).

Intravitreal injection of $MnCl_2$ is a common practice for MEMRI studies. The toxicity of intravitreal injection of $MnCl_2$ in mice and rats has been investigated previously (Bearer et al., 2007; Haenold et al., 2012; Luo et al., 2012; Thuen et al., 2008). In a preliminary study (Lin et al., 2014), we have concluded that intravitreal injection (0.25 μL of 0.2 M $MnCl_2$) slightly affected visual acuity with full recovery a day later without causing axonal injury or loss in C57BL/6 mice. Thus, the observed axonal transport deficit in EAE mice optic nerves is not likely an artifact resulting from $MnCl_2$ injection.

Why might axonal transport be affected in early inflammatory demyelination? Axonal transport depends on energy supplied by mitochondria (Ohno et al., 2011). In MS and its animal model EAE, several pathologies conspire to reduce energy supply. Nitric oxide and the free radical/reactive oxygen species are increased, including within axons, and inhibit mitochondrial function (Smith and Lassmann, 2002) reducing energy production. Sodium channel redistribution in demyelinated axons reduces internode length, thereby increasing the energy consumption needed for signal propagation (Dutta et al., 2006; Kornek et al., 2001; Waxman, 2006). The potential energy deficit would eventually lead to failure of the Na^+/K^+-ATPase pump (which requires energy for maintenance) and increased intracellular Na^+, thus triggering the reversal of Na^+/Ca^{2+} exchanger. The resultant influx and accumulation of intracellular Ca^{2+} may then lead to further mitochondrial dysfunction and axonal damage (Andrews et al., 2005; Craner et al., 2005; Mao and Reddy, 2010; Stys, 2005; Su et al., 2009). Excessive glutamate production by inflammatory cells, coupled with reduced buffering capacity of glial cells leads to glutamate-induced excitotoxicity of axons (which express glutamate receptors) (Mark et al., 2001; Pitt et al., 2000; Stys, 2005; Su et al., 2009; Trapp and Nave, 2008), results in inhibition of mitochondrial mobility and function (Macaskill et al., 2009; Rintoul et al., 2003). Therefore, a vicious cycle of disruption of ion homeostasis, energy deficits, and axonal transport deficits could play a crucial role in axonal degeneration (De Vos et al., 2008; Hollenbeck and Saxton, 2005; Mao and Reddy, 2010; Millecamps and Julien, 2013).

In this study, positive TUJ1 staining was applied (Fig. 5) to reflect βIII tubulin, associated with fast axonal transport of molecules and organelles (Jouhilahti et al., 2008; Niwa et al., 2013). Our data showed that accumulation and transport rates correlated well with TUJ1 staining results (Fig. 6B and C), supporting that MEMRI is appropriate for investigating axonal transport integrity in optic nerves. Although the current data are not sufficient to

determine whether the impaired axonal transport is the result or the cause of axonal injury at the onset of ON (Fig. 6D – 6I), its association with various axonal pathologies was apparent. Excess nitric oxide and reactive oxygen species are produced during neuroinflammation. These species have been shown to decrease axonal transport *in vitro* (Fang et al., 2012; Stagi et al., 2005). In other studies, excessive nitric oxide was shown to reversibly block impulse conduction in demyelinated CNS axons of rodents (Redford et al., 1997) while reduction in nitric oxide at the inflammation site prevented further axonal degeneration (Smith et al., 2001). Demyelination was also reported to result in axonal transport disruption in EAE mice (O'Neill et al., 1998; Rodriguez, 2003). Phosphorylated neurofilaments play a role in regulating axonal transport (Roy et al., 2000; Shea et al., 2003). Our current findings that decreased axonal transport correlated with reduced SMI-31 and MBP, and increased DAPI staining are consistent with these literature reports.

In summary, this study demonstrated the presence of impaired optic nerve axonal transport in the early stages of ON in EAE mice. The decreased axonal transport rate correlated with impaired visual function, diminished tubulins, and axonal pathologies including axonal injury, demyelination, and inflammation.

Acknowledgments

The authors thank Mr. Bob Mikesell for excellent technical assistance. This study was supported in part by the grants from National Institute of Health R01-NS047592 (S.-K.S.), P01-NS059560 (A.H.C.), National Multiple Sclerosis Society (NMSS) RG 4549A4/1 (S.-K.S.), and Department of Defense Ideal Award W81XWH-12-1-0457 (S.-K.S.).

Reference

Andrews HE, Nichols PP, Bates D, Turnbull DM. Mitochondrial dysfunction plays a key role in progressive axonal loss in Multiple Sclerosis. Med Hypotheses. 2005; 64:669–677. [PubMed: 15694681]

Bearer EL, Falzone TL, Zhang X, Biris O, Rasin A, Jacobs RE. Role of neuronal activity and kinesin on tract tracing by manganese-enhanced MRI (MEMRI). Neuroimage. 2007; 37(Suppl 1):S37–S46. [PubMed: 17600729]

Beck RW, Cleary PA, Trobe JD, Kaufman DI, Kupersmith MJ, Paty DW, Brown CH. The effect of corticosteroids for acute optic neuritis on the subsequent development of multiple sclerosis. The Optic Neuritis Study Group. N Engl J Med. 1993; 329:1764–1769. [PubMed: 8232485]

Beck RW, Trobe JD, Moke PS, Gal RL, Xing D, Bhatti MT, Brodsky MC, Buckley EG, Chrousos GA, Corbett J, Eggenberger E, Goodwin JA, Katz B, Kaufman DI, Keltner JL, Kupersmith MJ, Miller NR, Nazarian S, Orengo-Nania S, Savino PJ, Shults WT, Smith CH, Wall M. Optic Neuritis Study, G. High- and low-risk profiles for the development of multiple sclerosis within 10 years after optic neuritis: experience of the optic neuritis treatment trial. Arch Ophthalmol. 2003; 121:944–949. [PubMed: 12860795]

Bettelli E, Pagany M, Weiner HL, Linington C, Sobel RA, Kuchroo VK. Myelin oligodendrocyte glycoprotein-specific T cell receptor transgenic mice develop spontaneous autoimmune optic neuritis. J Exp Med. 2003; 197:1073–1081. [PubMed: 12732654]

Bitsch A, Schuchardt J, Bunkowski S, Kuhlmann T, Bruck W. Acute axonal injury in multiple sclerosis. Correlation with demyelination and inflammation. Brain. 2000; 123(Pt 6):1174–1183. [PubMed: 10825356]

Blewitt ES, Pogmore T, Talbot IC. Double embedding in agar/paraffin wax as an aid to orientation of mucosal biopsies. J Clin Pathol. 1982; 35:365. [PubMed: 7068930]

Boretius S, Gadjanski I, Demmer I, Bahr M, Diem R, Michaelis T, Frahm J. MRI of optic neuritis in a rat model. Neuroimage. 2008; 41:323–334. [PubMed: 18394926]

Budde MD, Xie M, Cross AH, Song SK. Axial diffusivity is the primary correlate of axonal injury in the experimental autoimmune encephalomyelitis spinal cord: a quantitative pixelwise analysis. J Neurosci. 2009; 29:2805–2813. [PubMed: 19261876]

Chan KC, Fu QL, Hui ES, So KF, Wu EX. Evaluation of the retina and optic nerve in a rat model of chronic glaucoma using in vivo manganese-enhanced magnetic resonance imaging. Neuroimage. 2008; 40:1166–1174. [PubMed: 18272401]

Chan KC, Li J, Kau P, Zhou IY, Cheung MM, Lau C, Yang J, So KF, Wu EX. In vivo retinotopic mapping of superior colliculus using manganese-enhanced magnetic resonance imaging. Neuroimage. 2011; 54:389–395. [PubMed: 20633657]

Chen J, Chiang CW, Zhang H, Song SK. Cell swelling contributes to thickening of low-dose N-methyl-D-aspartate-induced retinal edema. Invest Ophthalmol Vis Sci. 2012; 53:2777–2785. [PubMed: 22467578]

Chiang CW, Wang Y, Lin TH, Cross AH, Song SK. Acute visual function impairment in EAE is primarily caused by optic nerve inflammation as assessed by DBSI. Proc. Intl. Soc. Mag. Reson. Med. 2012; 20:3085.

Compston A, Coles A. Multiple sclerosis. Lancet. 2008; 372:1502–1517. [PubMed: 18970977]

Craner MJ, Damarjian TG, Liu S, Hains BC, Lo AC, Black JA, Newcombe J, Cuzner ML, Waxman SG. Sodium channels contribute to microglia/macrophage activation and function in EAE and MS. Glia. 2005; 49:220–229. [PubMed: 15390090]

Cross DJ, Flexman JA, Anzai Y, Maravilla KR, Minoshima S. Age-related decrease in axonal transport measured by MR imaging in vivo. Neuroimage. 2008; 39:915–926. [PubMed: 17980625]

De Vos KJ, Grierson AJ, Ackerley S, Miller CC. Role of axonal transport in neurodegenerative diseases. Annu Rev Neurosci. 2008; 31:151–173. [PubMed: 18558852]

Diem R, Demmer I, Boretius S, Merkler D, Schmelting B, Williams SK, Sattler MB, Bahr M, Michaelis T, Frahm J, Bruck W, Fuchs E. Autoimmune optic neuritis in the common marmoset monkey: comparison of visual evoked potentials with MRI and histopathology. Invest Ophthalmol Vis Sci. 2008; 49:3707–3714. [PubMed: 18450589]

Dutta R, McDonough J, Yin X, Peterson J, Chang A, Torres T, Gudz T, Macklin WB, Lewis DA, Fox RJ, Rudick R, Mirnics K, Trapp BD. Mitochondrial dysfunction as a cause of axonal degeneration in multiple sclerosis patients. Ann Neurol. 2006; 59:478–489. [PubMed: 16392116]

Fairless R, Williams SK, Hoffmann DB, Stojic A, Hochmeister S, Schmitz F, Storch MK, Diem R. Preclinical retinal neurodegeneration in a model of multiple sclerosis. J Neurosci. 2012; 32:5585–5597. [PubMed: 22514320]

Fang C, Bourdette D, Banker G. Oxidative stress inhibits axonal transport: implications for neurodegenerative diseases. Mol Neurodegener. 2012; 7:29. [PubMed: 22709375]

Ferguson B, Matyszak MK, Esiri MM, Perry VH. Axonal damage in acute multiple sclerosis lesions. Brain. 1997; 120(Pt 3):393–399. [PubMed: 9126051]

Gadjanski I, Boretius S, Williams SK, Lingor P, Knoferle J, Sattler MB, Fairless R, Hochmeister S, Suhs KW, Michaelis T, Frahm J, Storch MK, Bahr M, Diem R. Role of n-type voltage-dependent calcium channels in autoimmune optic neuritis. Ann Neurol. 2009; 66:81–93. [PubMed: 19670438]

Gold R, Linington C, Lassmann H. Understanding pathogenesis and therapy of multiple sclerosis via animal models: 70 years of merits and culprits in experimental autoimmune encephalomyelitis research. Brain. 2006; 129:1953–1971. [PubMed: 16632554]

Guy J. MRI in experimental inflammatory and mitochondrial optic neuropathies. NMR Biomed. 2008; 21:968–977. [PubMed: 18756439]

Haenold R, Herrmann KH, Schmidt S, Reichenbach JR, Schmidt KF, Lowel S, Witte OW, Weih F, Kretz A. Magnetic resonance imaging of the mouse visual pathway for in vivo studies of degeneration and regeneration in the CNS. Neuroimage. 2012; 59:363–376. [PubMed: 21835252]

Hickman SJ, Toosy AT, Jones SJ, Altmann DR, Miszkiel KA, MacManus DG, Barker GJ, Plant GT, Thompson AJ, Miller DH. A serial MRI study following optic nerve mean area in acute optic neuritis. Brain. 2004; 127:2498–2505. [PubMed: 15342363]

Hollenbeck PJ, Saxton WM. The axonal transport of mitochondria. J Cell Sci. 2005; 118:5411–5419. [PubMed: 16306220]

Jevtovic-Todorovic V, Absalom AR, Blomgren K, Brambrink A, Crosby G, Culley DJ, Fiskum G, Giffard RG, Herold KF, Loepke AW, Ma D, Orser BA, Planel E, Slikker W Jr, Soriano SG, Stratmann G, Vutskits L, Xie Z, Hemmings HC Jr. Anaesthetic neurotoxicity and neuroplasticity: an expert group report and statement based on the BJA Salzburg Seminar. Br J Anaesth. 2013

Jouhilahti EM, Peltonen S, Peltonen J. Class III beta-tubulin is a component of the mitotic spindle in multiple cell types. J Histochem Cytochem. 2008; 56:1113–1119. [PubMed: 18796406]

Kameyama K, Aono K, Kitamura K. Isoflurane inhibits neuronal Ca2+ channels through enhancement of current inactivation. Br J Anaesth. 1999; 82:402–411. [PubMed: 10434825]

Kornek B, Storch MK, Bauer J, Djamshidian A, Weissert R, Wallstroem E, Stefferl A, Zimprich F, Olsson T, Linington C, Schmidbauer M, Lassmann H. Distribution of a calcium channel subunit in dystrophic axons in multiple sclerosis and experimental autoimmune encephalomyelitis. Brain. 2001; 124:1114–1124. [PubMed: 11353727]

Leergaard TB, Bjaalie JG, Devor A, Wald LL, Dale AM. In vivo tracing of major rat brain pathways using manganese-enhanced magnetic resonance imaging and threedimensional digital atlasing. Neuroimage. 2003; 20:1591–1600. [PubMed: 14642470]

Lin TH, Chiang CW, Trinkaus K, Spees WM, Sun P, Song SK. Manganeseenhanced MRI (MEMRI) via topical loading of Mn(2+) significantly impairs mouse visual acuity: a comparison with intravitreal injection. NMR Biomed. 2014; 27:390–398. [PubMed: 24436112]

Linker RA, Lee DH, Demir S, Wiese S, Kruse N, Siglienti I, Gerhardt E, Neumann H, Sendtner M, Luhder F, Gold R. Functional role of brain-derived neurotrophic factor in neuroprotective autoimmunity: therapeutic implications in a model of multiple sclerosis. Brain. 2010; 133:2248–2263. [PubMed: 20826430]

Luo L, Xu H, Li Y, Du Z, Sun X, Ma Z, Hu Y. Manganese-enhanced MRI optic nerve tracking: effect of intravitreal manganese dose on retinal toxicity. NMR in biomedicine. 2012

Macaskill AF, Rinholm JE, Twelvetrees AE, Arancibia-Carcamo IL, Muir J, Fransson A, Aspenstrom P, Attwell D, Kittler JT. Miro1 is a calcium sensor for glutamate receptor-dependent localization of mitochondria at synapses. Neuron. 2009; 61:541–555. [PubMed: 19249275]

MacKenzie-Graham AJ, Rinek GA, Avedisian A, Morales LB, Umeda E, Boulat B, Jacobs RE, Toga AW, Voskuhl RR. Estrogen treatment prevents gray matter atrophy in experimental autoimmune encephalomyelitis. J Neurosci Res. 2012; 90:1310–1323. [PubMed: 22411609]

Mao PZ, Reddy PH. Is multiple sclerosis a mitochondrial disease? Biochimica Et Biophysica Acta-Molecular Basis of Disease. 2010; 1802:66–79.

Mark LP, Prost RW, Ulmer JL, Smith MM, Daniels DL, Strottmann JM, Brown WD, Hacein-Bey L. Pictorial review of glutamate excitotoxicity: fundamental concepts for neuroimaging. AJNR Am J Neuroradiol. 2001; 22:1813–1824. [PubMed: 11733308]

Massaad CA, Amin SK, Hu L, Mei Y, Klann E, Pautler RG. Mitochondrial superoxide contributes to blood flow and axonal transport deficits in the Tg2576 mouse model of Alzheimer's disease. PLoS One. 2010; 5:e10561. [PubMed: 20479943]

Millecamps S, Julien JP. Axonal transport deficits and neurodegenerative diseases. Nat Rev Neurosci. 2013; 14:161–176. [PubMed: 23361386]

Niwa S, Takahashi H, Hirokawa N. beta-Tubulin mutations that cause severe neuropathies disrupt axonal transport. EMBO J. 2013; 32:1352–1364. [PubMed: 23503589]

O'Neill JK, Baker D, Morris MM, Gschmeissner SE, Jenkins HG, Butt AM, Kirvell SL, Amor S. Optic neuritis in chronic relapsing experimental allergic encephalomyelitis in Biozzi ABH mice: demyelination and fast axonal transport changes in disease. J Neuroimmunol. 1998; 82:210–218. [PubMed: 9585818]

Ohno N, Kidd GJ, Mahad D, Kiryu-Seo S, Avishai A, Komuro H, Trapp BD. Myelination and axonal electrical activity modulate the distribution and motility of mitochondria at CNS nodes of Ranvier. J Neurosci. 2011; 31:7249–7258. [PubMed: 21593309]

Olsen O, Kristoffersen A, Thuen M, Sandvig A, Brekken C, Haraldseth O, Goa PE. Manganese transport in the rat optic nerve evaluated with spatial- and time-resolved magnetic resonance imaging. J Magn Reson Imaging. 2010; 32:551–560. [PubMed: 20815052]

Pascual AM, Tellez N, Bosca I, Mallada J, Belenguer A, Abellan I, Sempere AP, Fernandez P, Magraner MJ, Coret F, Sanz MA, Montalban X, Casanova B. Revision of the risk of secondary

leukaemia after mitoxantrone in multiple sclerosis populations is required. Mult Scler. 2009; 15:1303–1310. [PubMed: 19825889]

Pautler RG, Koretsky AP. Tracing odor-induced activation in the olfactory bulbs of mice using manganese-enhanced magnetic resonance imaging. Neuroimage. 2002; 16:441–448. [PubMed: 12030829]

Pautler RG, Silva AC, Koretsky AP. In vivo neuronal tract tracing using manganeseenhanced magnetic resonance imaging. Magn Reson Med. 1998; 40:740–748. [PubMed: 9797158]

Petratos S, Ozturk E, Azari MF, Kenny R, Lee JY, Magee KA, Harvey AR, McDonald C, Taghian K, Moussa L, Mun Aui P, Siatskas C, Litwak S, Fehlings MG, Strittmatter SM, Bernard CC. Limiting multiple sclerosis related axonopathy by blocking Nogo receptor and CRMP-2 phosphorylation. Brain. 2012; 135:1794–1818. [PubMed: 22544872]

Pitt D, Werner P, Raine CS. Glutamate excitotoxicity in a model of multiple sclerosis. Nat Med. 2000; 6:67–70. [PubMed: 10613826]

Redford EJ, Kapoor R, Smith KJ. Nitric oxide donors reversibly block axonal conduction: demyelinated axons are especially susceptible. Brain. 1997; 120(Pt 12):2149–2157. [PubMed: 9448570]

Ridder WH 3rd, Nusinowitz S. The visual evoked potential in the mouse--origins and response characteristics. Vision Res. 2006; 46:902–913. [PubMed: 16242750]

Rintoul GL, Filiano AJ, Brocard JB, Kress GJ, Reynolds IJ. Glutamate decreases mitochondrial size and movement in primary forebrain neurons. The Journal of neuroscience : the official journal of the Society for Neuroscience. 2003; 23:7881–7888. [PubMed: 12944518]

Rodriguez M. A function of myelin is to protect axons from subsequent injury: implications for deficits in multiple sclerosis. Brain. 2003; 126:751–752. [PubMed: 12615635]

Roy S, Coffee P, Smith G, Liem RK, Brady ST, Black MM. Neurofilaments are transported rapidly but intermittently in axons: implications for slow axonal transport. J Neurosci. 2000; 20:6849–6861. [PubMed: 10995829]

Saleem KS, Pauls JM, Augath M, Trinath T, Prause BA, Hashikawa T, Logothetis NK. Magnetic resonance imaging of neuronal connections in the macaque monkey. Neuron. 2002; 34:685–700. [PubMed: 12062017]

Sally JD, Sally PJ. Roots to research : a vertical development of mathematical problems. American Mathematical Society, Providence, R.I. 2007

Schneider CA, Rasband WS, Eliceiri KW. NIH Image to ImageJ: 25 years of image analysis. Nat Methods. 2012; 9:671–675. [PubMed: 22930834]

Shams PN, Plant GT. Optic neuritis: a review. Int MS J. 2009; 16:82–89. [PubMed: 19878630]

Shao H, Huang Z, Sun SL, Kaplan HJ, Sun D. Myelin/oligodendrocyte glycoprotein-specific T-cells induce severe optic neuritis in the C57BL/6 mouse. Invest Ophthalmol Vis Sci. 2004; 45:4060–4065. [PubMed: 15505056]

Sharma R, Buras E, Terashima T, Serrano F, Massaad CA, Hu L, Bitner B, Inoue T, Chan L, Pautler RG. Hyperglycemia induces oxidative stress and impairs axonal transport rates in mice. PLoS One. 2010; 5:e13463. [PubMed: 20976160]

Shea TB, Jung C, Pant HC. Does neurofilament phosphorylation regulate axonal transport? Trends Neurosci. 2003; 26:397–400. [PubMed: 12900166]

Silva AC, Lee JH, Aoki I, Koretsky AP. Manganese-enhanced magnetic resonance imaging (MEMRI): methodological and practical considerations. NMR Biomed. 2004; 17:532–543. [PubMed: 15617052]

Smith DH, Chen XH, Iwata A, Graham DI. Amyloid beta accumulation in axons after traumatic brain injury in humans. J Neurosurg. 2003; 98:1072–1077. [PubMed: 12744368]

Smith KD, Kallhoff V, Zheng H, Pautler RG. In vivo axonal transport rates decrease in a mouse model of Alzheimer's disease. Neuroimage. 2007; 35:1401–1408. [PubMed: 17369054]

Smith KJ, Kapoor R, Hall SM, Davies M. Electrically active axons degenerate when exposed to nitric oxide. Ann Neurol. 2001; 49:470–476. [PubMed: 11310624]

Smith KJ, Lassmann H. The role of nitric oxide in multiple sclerosis. Lancet Neurol. 2002; 1:232–241. [PubMed: 12849456]

Song SK, Sun SW, Ju WK, Lin SJ, Cross AH, Neufeld AH. Diffusion tensor imaging detects and differentiates axon and myelin degeneration in mouse optic nerve after retinal ischemia. Neuroimage. 2003; 20:1714–1722. [PubMed: 14642481]

Stagi M, Dittrich PS, Frank N, Iliev AI, Schwille P, Neumann H. Breakdown of axonal synaptic vesicle precursor transport by microglial nitric oxide. J Neurosci. 2005; 25:352–362. [PubMed: 15647478]

Stys PK. General mechanisms of axonal damage and its prevention. J Neurol Sci. 2005; 233:3–13. [PubMed: 15899499]

Su KG, Banker G, Bourdette D, Forte M. Axonal degeneration in multiple sclerosis: the mitochondrial hypothesis. Curr Neurol Neurosci Rep. 2009; 9:411–417. [PubMed: 19664372]

Sun SW, Liang HF, Schmidt RE, Cross AH, Song SK. Selective vulnerability of cerebral white matter in a murine model of multiple sclerosis detected using diffusion tensor imaging. Neurobiol Dis. 2007; 28:30–38. [PubMed: 17683944]

Thuen M, Berry M, Pedersen TB, Goa PE, Summerfield M, Haraldseth O, Sandvig A, Brekken C. Manganese-enhanced MRI of the rat visual pathway: acute neural toxicity, contrast enhancement, axon resolution, axonal transport, and clearance of Mn(2+). J Magn Reson Imaging. 2008; 28:855–865. [PubMed: 18821627]

Trapp BD, Nave KA. Multiple sclerosis: an immune or neurodegenerative disorder? Annu Rev Neurosci. 2008; 31:247–269. [PubMed: 18558855]

Van der Linden A, Verhoye M, Van Meir V, Tindemans I, Eens M, Absil P, Balthazart J. In vivo manganese-enhanced magnetic resonance imaging reveals connections and functional properties of the songbird vocal control system. Neuroscience. 2002; 112:467–474. [PubMed: 12044464]

Wang FH, Appelkvist P, Klason T, Gissberg O, Bogstedt A, Eliason K, Martinsson S, Briem S, Andersson A, Visser SA, Ivarsson M, Lindberg M, Agerman K, Sandin J. Decreased axonal transport rates in the Tg2576 APP transgenic mouse: improvement with the gamma-secretase inhibitor MRK-560 as detected by manganese-enhanced MRI. Eur J Neurosci. 2012; 36:3165–3172. [PubMed: 22958226]

Wang Y, Wang Q, Haldar JP, Yeh FC, Xie M, Sun P, Tu TW, Trinkaus K, Klein RS, Cross AH, Song SK. Quantification of increased cellularity during inflammatory demyelination. Brain. 2011; 134:3590–3601. [PubMed: 22171354]

Watanabe T, Frahm J, Michaelis T. Functional mapping of neural pathways in rodent brain in vivo using manganese-enhanced three-dimensional magnetic resonance imaging. NMR Biomed. 2004; 17:554–568. [PubMed: 15617054]

Waxman SG. Axonal conduction and injury in multiple sclerosis: the role of sodium channels. Nat Rev Neurosci. 2006; 7:932–941. [PubMed: 17115075]

Highlights

- Optic nerve axonal transport rate was quantified using MEMRI
- Axonal transport rate significantly decreased at the onset of optic neuritis
- Decreased axonal transport rates correlated with axonal pathologies
- Decreased axonal transport rate correlated with visual acuity

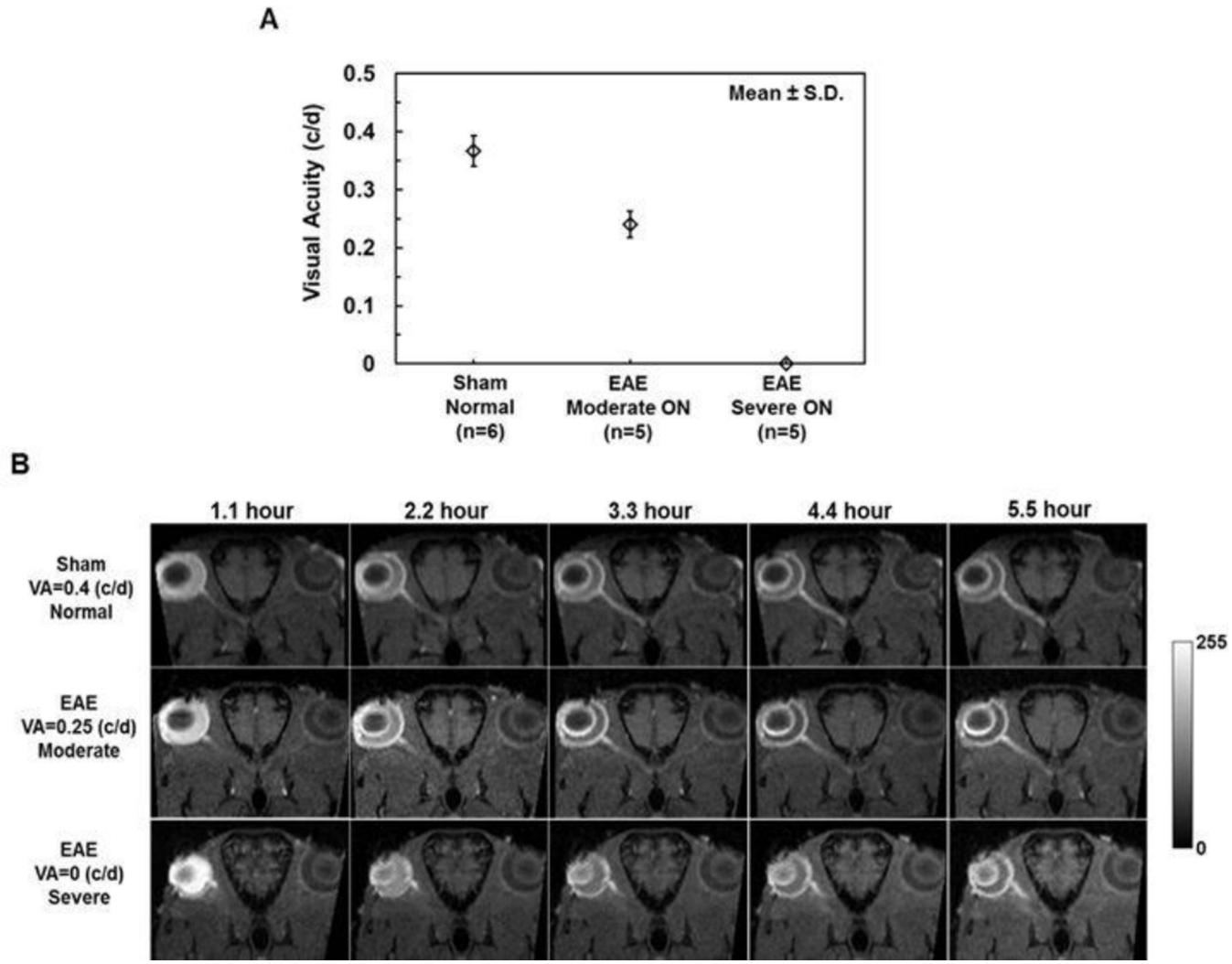

Figure 1.

Group averaged visual acuity (VA) of sham (n=6) and EAE (n=10) eyes before MEMRI experiments. EAE mice were grouped based on VA to moderate (VA = 0.25/0.20 c/d) and severe (VA = 0 c/d) ON groups (A). A serial time-lapse oblique corrected T1W images from representative mice are presented to demonstrate the different degree of Mn^{2+}-enhancement of optic nerves from sham and EAE mice from 1.1 – 5.5 hours post-injection (B). Mn^{2+}-enhancement of optic nerves clearly increases with time. At the end time point, mice with the lower VA exhibited less Mn^{2+}-enhancement reflecting slower axonal transport.

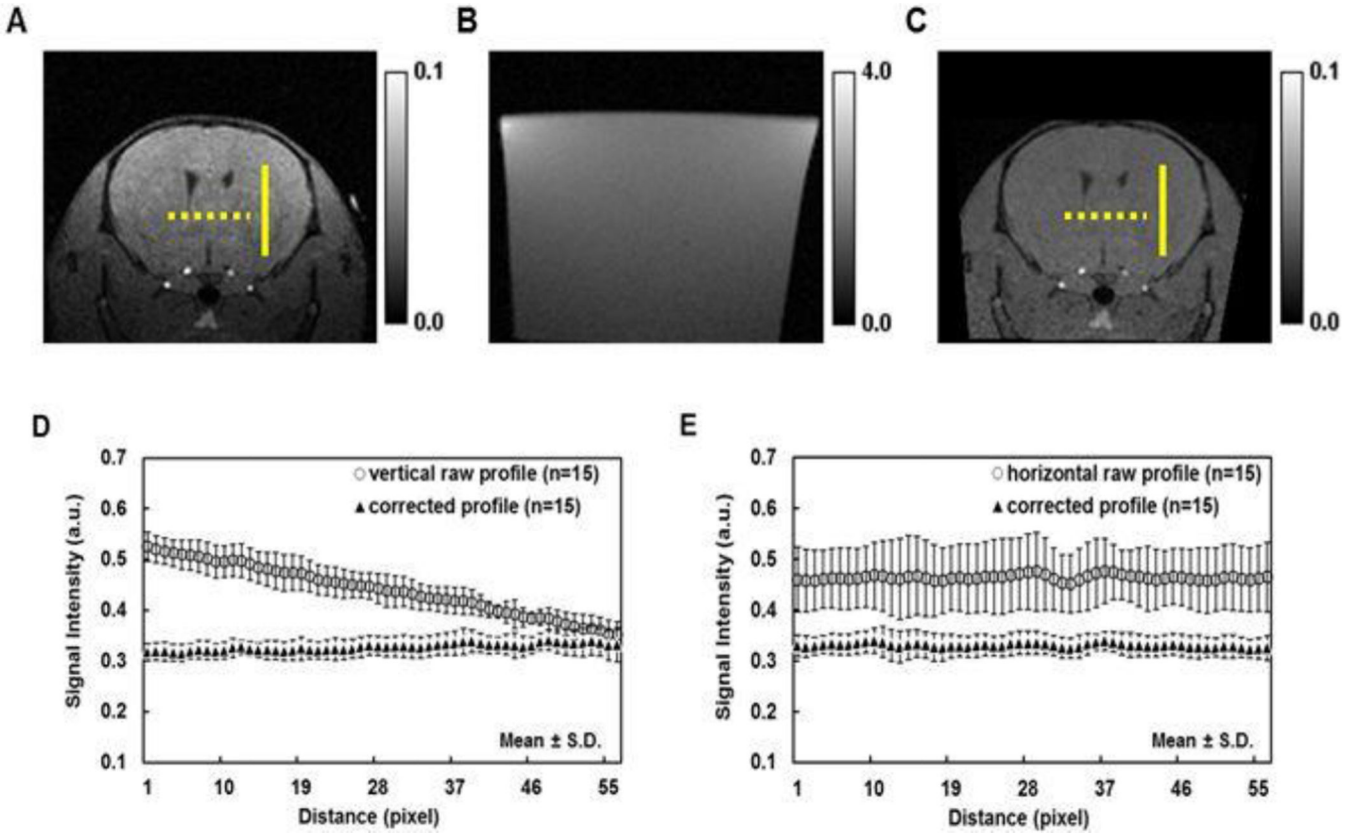

Figure 2.

A T1W image of 2% agar gel was used to compensate the B1-inhomogeneity effect in the raw data set generating the corrected T1W images. Three representative images are raw T1W image of mouse brain (A), T1W image of 2% agar gel (B), and the corresponding corrected T1W image (C), which was generated from raw T1W image of mouse brain (A) divided by T1W image of 2% agar gel (B) voxel by voxel. Three vertical (solid lines, A and C) and three horizontal (round dots, A and C) profiles were randomly drawn in each of five mouse-brain images of raw and corrected T1W, respectively. The group averaged raw profile showed linear decrease from top to bottom in vertical orientation (D). Even though there is no obviously variation with the profile from left to right in horizontal orientation, the intensity value is highly layer-dependence (E). The corrected vertical and horizontal profiles were stable (D and E) and suggested that B1 inhomogeneity was compensated successfully.

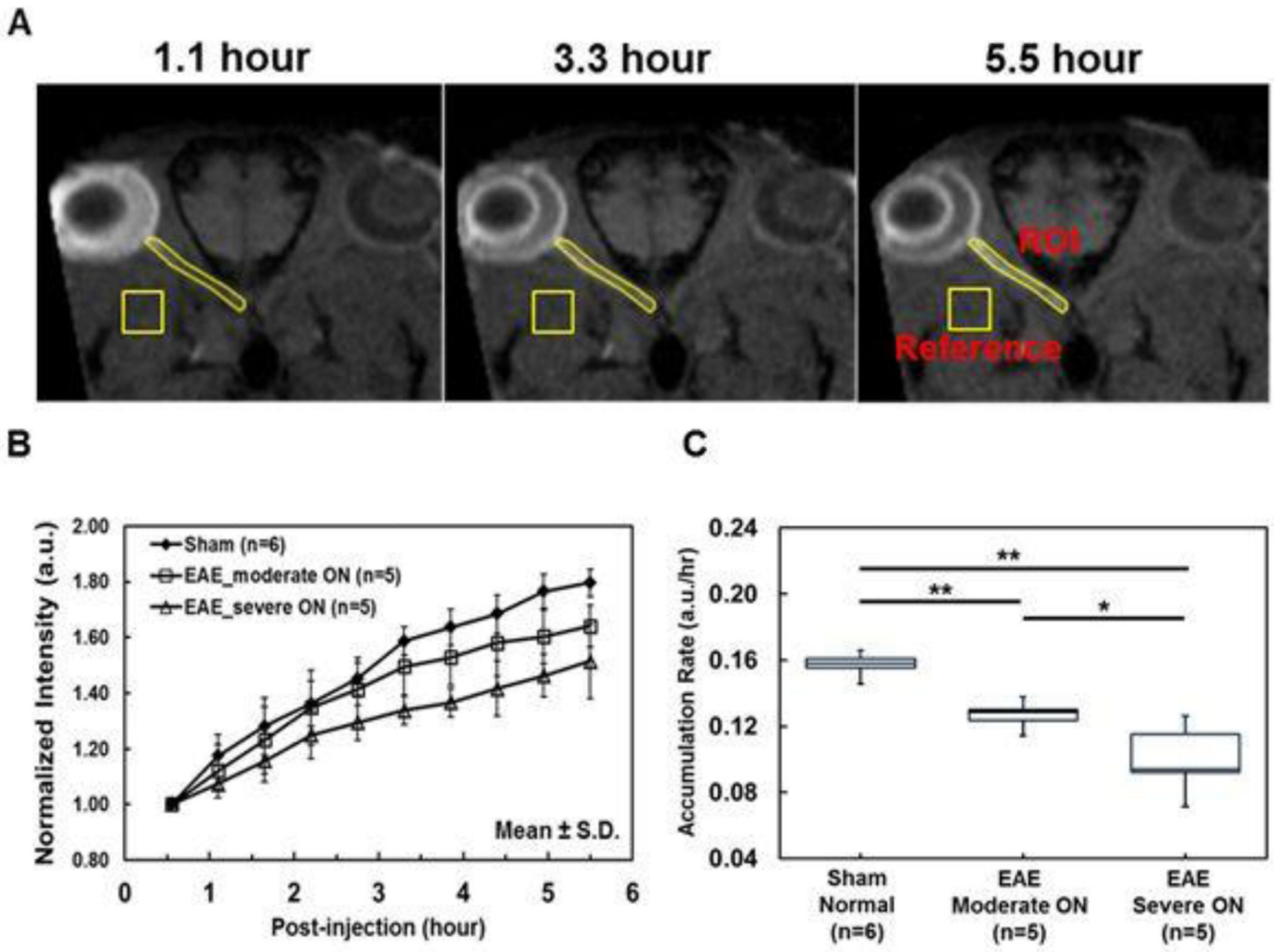

Figure 3.

The ROI of optic nerve and reference area of muscle, where Mn^{2+} does not reach, were defined on the corrected T1W oblique image at each time point (A). The group average of the normalized optic nerve signal intensity from sham, moderate ON and severe ON mice was obtained for each time point from 0.55 – 5.5 hours after injection at a 0.55 hours resolution. The higher rate of Mn^{2+} accumulation over time was associated with the better VA (B). The group averaged slope of the normalized signal intensity over time was defined as the optic nerve accumulation rate of total Mn^{2+}. The box plots reveal that Mn^{2+}accumulation rate of severe ON optic nerves was slower than that of the moderate ON nerves, which was slower than that of the same nerves (B and C).

* indicates $p < 0.05$

** indicates $p < 0.005$

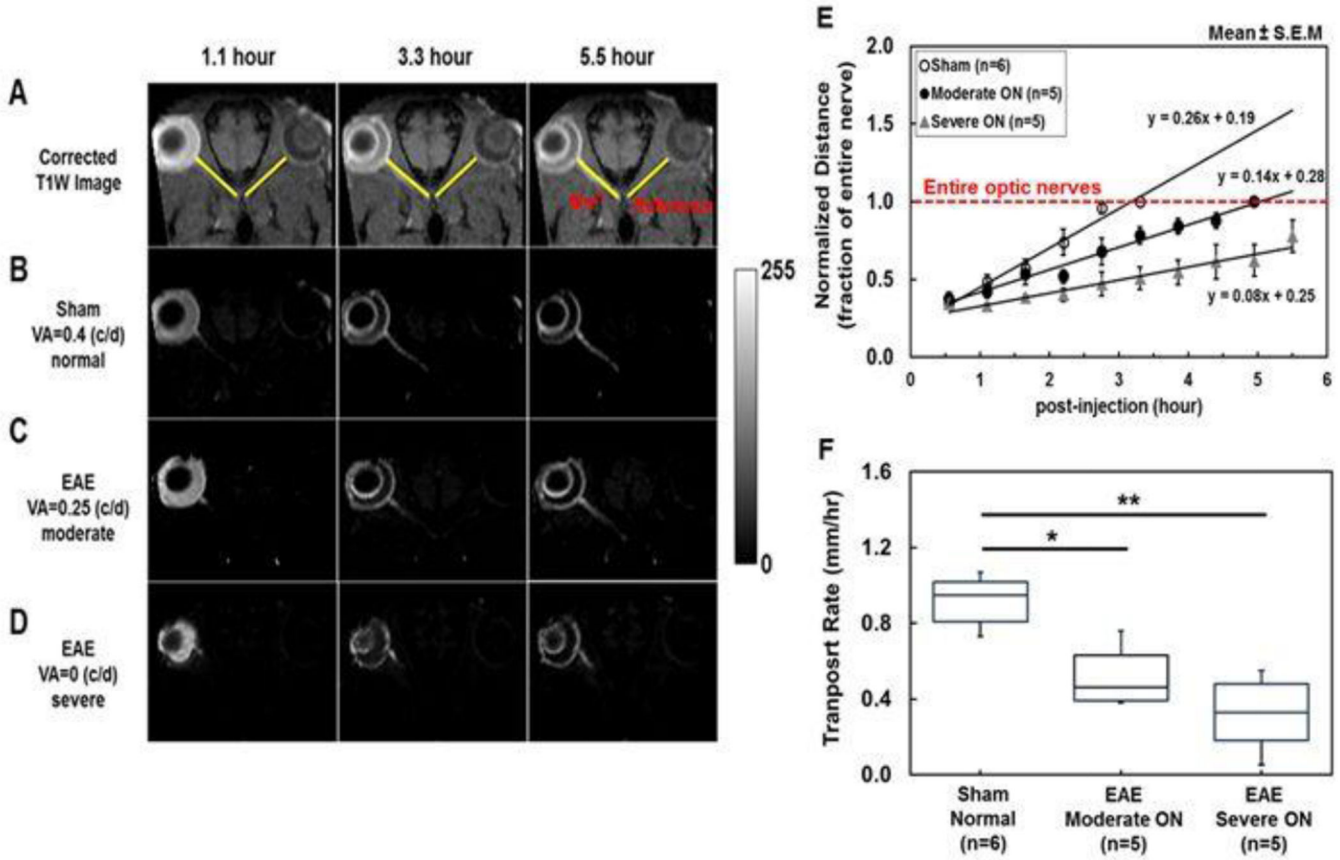

Figure 4.

To estimate Mn^{2+} transport rate in mm/hour, line-ROIs were defined to match the optic nerve length (A). The arrival of Mn^{2+} in optic nerves was defined by the T1W enhancement of the optic nerves referencing to the line-ROI of the non-loaded eye. To visualize the extent of Mn^{2+}-enhancement, representative oblique-corrected T1W images from each group were displayed after subtracting the mean intensity of the reference line-ROI (B, C, and D). Three representative subtracted images of sham, moderate ON and severe ON mice (VA = 0.4, 0.25, and 0, respectively) show different degree of Mn^{2+} transport at 1.1, 3.3, and 5.5 hours post-injection (B, C, and D). For quantification of the transport rate, the arrival of Mn^{2+} was determined using **non-subtracted** images at each time point by identifying line-ROI voxels of the loaded eye with intensity higher than two standard deviation of the mean from the reference line-ROI of the non-loaded eye. The group averaged displacements, normalized to the total number of voxels of each nerve (red line, panel E), of Mn^{2+} over time revealed different rate of Mn^{2+} transport among the three groups of mice examined (E). Box plot shows transport rate distribution of each group in mm/hour by converting normalized voxel displacement to mm (F). The results demonstrated that Mn^{2+} transport rate of sham optic nerves were significantly faster than moderated ON ($p < 0.005$) and severe ON ($p < 0.005$) suggesting the presence of axonal transport impairment at the onset of ON in EAE mice.

* indicates $p < 0.05$

** indicates $p < 0.005$

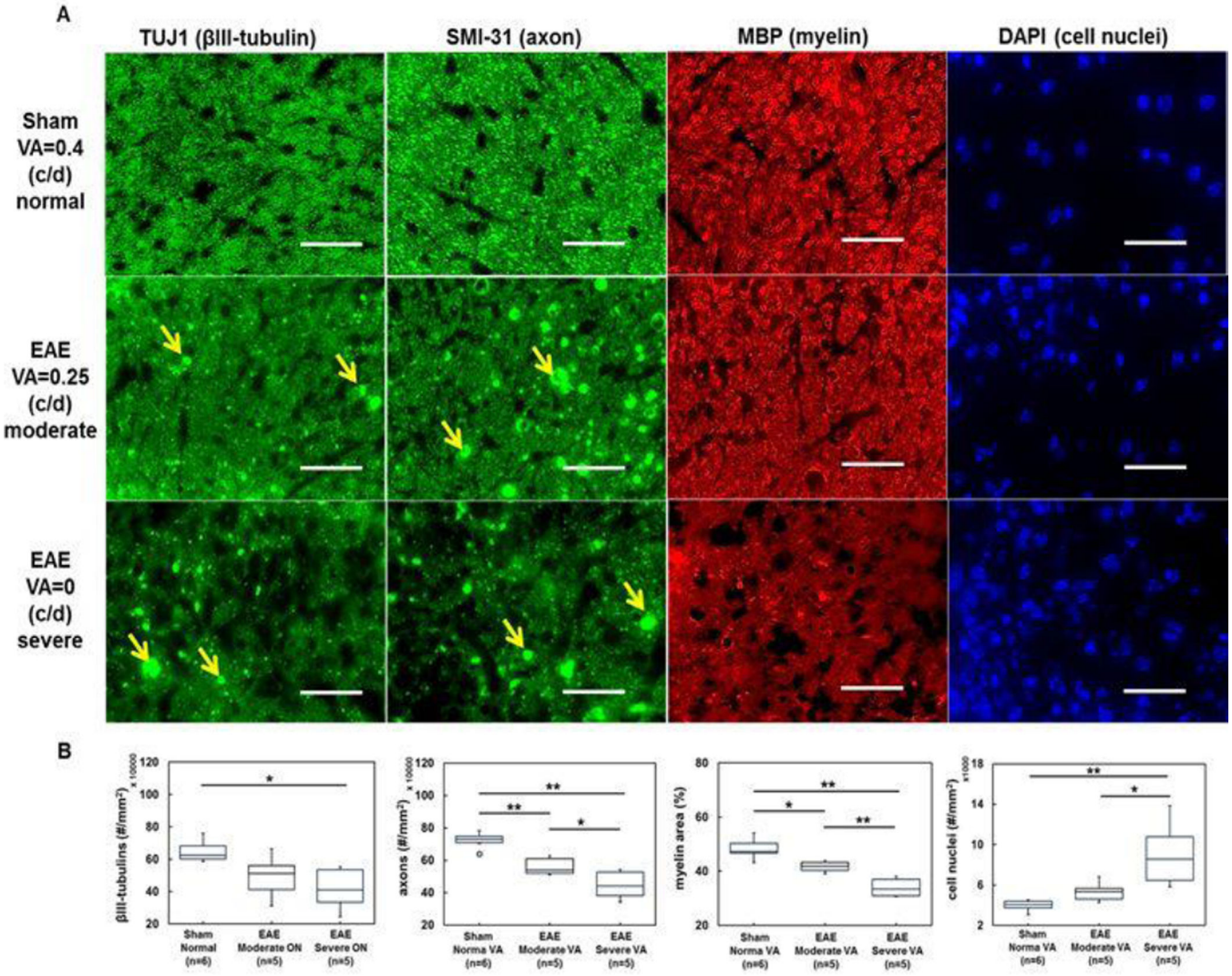

Figure 5.

Representative immunohistochemical staining of optic nerves from sham, moderate ON and severe ON mice (A). Images displayed are 56% field-of-view from the 60× magnification of mictrotubule-associated βIII-tubulin (TUJ1, green), phosphorylated neurofilament (SMI-31, green), myelin basic protein (MBP, red), and 4', 6-dianidino-2-phenylindole (DAPI, blue). Reduced density of TUJ1 (microtubulins) and SMI-31 (phosphorylated neurofilaments) positive axons were seen in optic nerve from moderate and severe ON mice. Areas of increased TUJ1 and SMI-31 positive patches were observed with increased severity of VA, probably reflecting axonal beading or debris (A, yellow arrows). Decreased density of MBP positive axons and increased DAPI positive nuclear staining was also seen with increased VA impairment. Box plots demonstrate the difference in axonal pathologies among the three groups examined (B).

Scale Bar: 25 μm

*$p < 0.05$

**$p < 0.005$

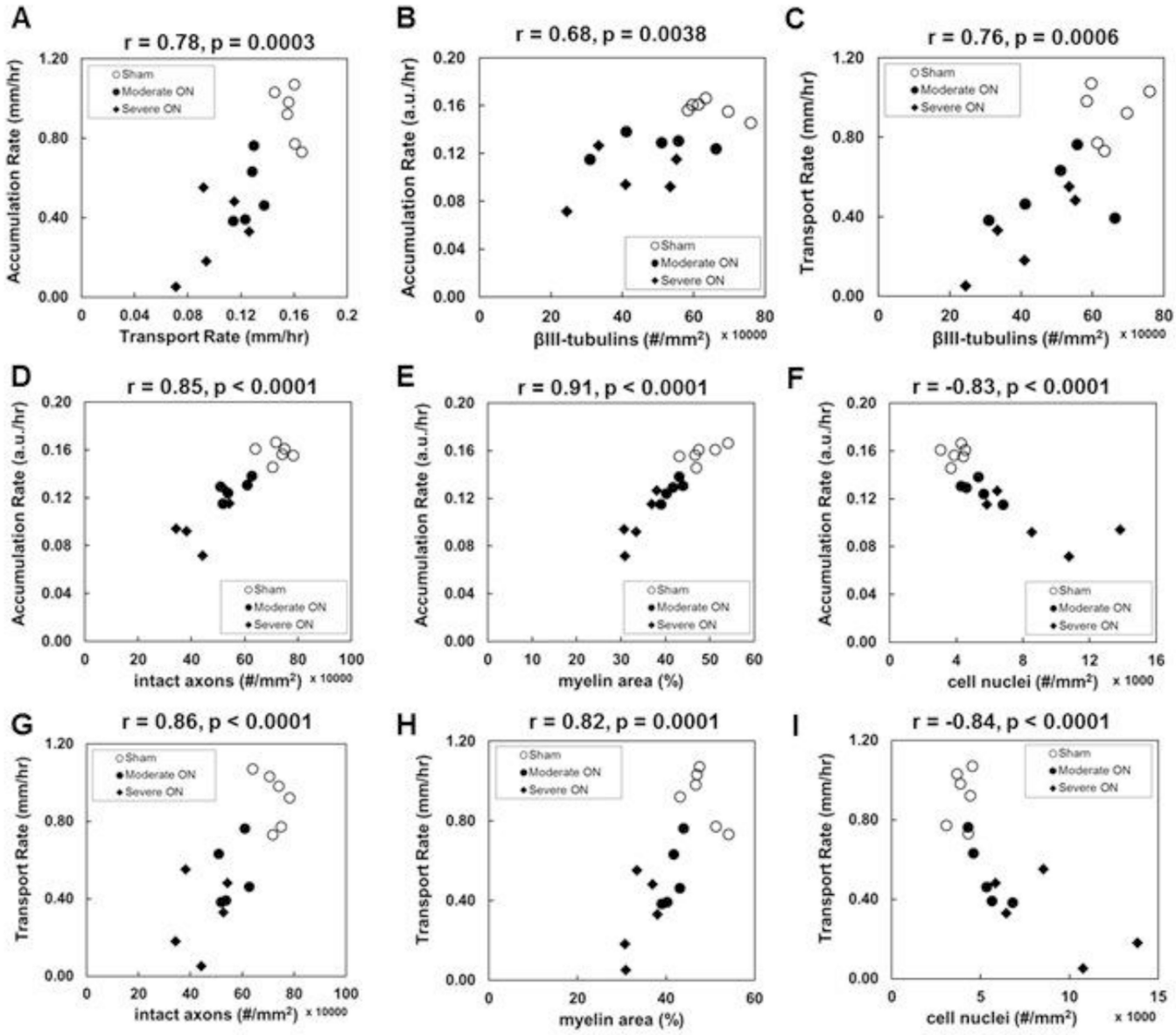

Figure 6.

Table 1

Group averaged accumulation and transport rates of sham (n=6), moderate ON (n=5) and severe ON (n=5)

	Sham (n=6)	Moderate ON (n=5)	Moderate ON (n=5)
Accumulation Rate	0.16 ± 0.01	0.13 ± 0.01	0.10 ± 0.02
Transport Rate	0.92 ± 0.14	0.52 ± 0.17	0.32 ± 0.21

Accumulation Rate (a.u./hour): mean ± S.D.

Transport Rate (mm/hour): mean ± S.D.